Mechanics of Advanced Composite Structures 5 (2018) 131 - 139

Semnan University

Mechanics of Advanced Composite Structures

journal homepage: http://MACS.journals.semnan.ac.ir

Effects of reinforcement distribution on the mechanical properties of Al–Fe_3O_4 nanocomposites fabricated via accumulative roll bonding

B. Pirouzi, E. Borhani*

Department of Nanotechnology, Nanomaterial Science group, Semnan University, 35131-19111, Semnan, Iran

PAPER INFO

Paper history:
Received 2017-08-22
Received in revised form 2018-01-07
Accepted 2018-07-14

Keywords:
Metal matrix composite
Fe_3O_4
Accumulative roll bonding
Microstructure
Mechanical properties
Fractography

ABSTRACT

This research developed new nanostructured Al–Fe_3O_4 composites via accumulative roll bonding (ARB). X-ray diffraction (XRD) analysis and field emission scanning electron microscopy were conducted to examine microstructural characteristics and particle distribution in the nanocomposites. Hardness and tensile strength tests were employed to examine their mechanical properties. After eight cycles of XRD analysis, the size of the Al crystals in the nanocomposites reached 198 nm. After eight cycles of tests on mechanical properties, the Al crystals exhibited a tensile strength and a hardness of 204 MPa and 63 HV, respectively. These values are higher than those achieved by pure Al. The depth of nanocomposite rupture observed in fractographic analysis revealed that a ductile fracture occurred in the materials because of the formation and growth of cavities.

1. Introduction

Metal matrix composites reinforced with nanoparticles have become one of the materials of interest to many researchers in recent decades [1–3]. These materials are used in industries, such as the aerospace, automotive, and electrical sectors. For these composites, designers and engineers have considered the use of Al alloy as a constituent because of its attractive characteristics, including low weight and affordable price. However, the application of Al in this regard has been restricted by the metal's poor strength and low elastic modulus. This problem prompted researchers to use a variety of composite fabrication methods to develop Al matrix composites reinforced with nanoparticles of high specific strength and stiffness [4, 5]. Metal matrix composites are produced through different approaches. One such approach is severe plastic deformation (SPD), which involves the application of high strain to produce nanoparticle-reinforced metal matrix composites without thermal operation, thus resulting in the formation of ultrafine-grained (UFG) structures. A type of SPD is accumulative roll bonding (ARB), which enables the accumulation of a very large strain in a material without changing the material's initial dimensions [6, 7]. This method requires the use of metal plates that are stacked after surface preparation and rolled under a strain of about 50%. The rolled product is split and stacked repeatedly in alternating cycles [8]. Using ARB to fabricate an Al matrix reinforced with various substances creates high-strength composites, including Al/Sc [6, 7], Al–ZrO_2 [9], Al–Al_2O_3 [10], and Al–SiC [11].

Depending on the type, size, shape, and distribution of reinforcement particles, different physical and mechanical properties are observed in composites.

* Corresponding author. Tel/Fax: +98-233-3354119
E-mail address: E.Borhani@Semnan.ac.ir
DOI: 10.22075/MACS.2018.12290.1121

For example, iron oxide Fe_3O_4 nanoparticles improve the magnetic properties of a composite and simultaneously increase its magnetic permeability, electrical conductivity, and thermal conductivity [12, 13]. Studies have explored Al–Fe_3O_4 nanocomposites manufactured via powder metallurgy and examined their magnetic permeability and hardness [14, 15]. In the current work, Al matrix nanocomposites reinforced with iron oxide Fe_3O_4 nanoparticles were produced through ARB, and the structural, microstructural, and mechanical properties of the nanocomposites were investigated.

2. Experimental procedure

The chemical composition and some of the mechanical properties of the annealed pure Al sheets used in this work are shown in Table 1. The Al sheets were cut into 250 mm × 50 mm × 1 mm panels to serve as the matrix of the nanocomposites. The panels were then annealed at 350○C for 1 h. Spherical Fe_3O_4 particles with an average size of 90 nm were used as reinforcement additives (Fig. 1). To fabricate the composites via the ARB process, the specimens were degreased in an acetone bath and scratch-brushed using a circular stainless steel brush. The Fe_3O_4 nanoparticles were suspended in acetone, and the resultant mixture was sprayed onto the aluminum strips with an atomizer. The strips were rolled to reduce their size by 50%. Subsequently, the rolled sheets were cut in half, degreased, stacked, and rolled without the addition of more particles. The final step was repeated up to eight ARB cycles at room temperature to achieve a mostly uniform distribution of reinforcement particles.

To examine the microstructure and distribution of nanoparticles, field emission scanning electron microscopy (FESEM) and X-ray diffraction (XRD) analysis were performed. The XRD analysis was carried out at a scanning mode of 25° to 90° and a step size of 0.05° at room temperature using Cu Kα radiation (λ=0.1542nm). With an Instron 550, tensile strength tests were conducted at various ARB cycles at a nominal strain rate of 8.3×10−4 S−1 under ambient temperature. Specimens with a gauge length and a width equal to 25 and 6 mm, respectively, were prepared in accordance with ASTM E8. The total elongation of the specimens was measured on the basis of the difference in gauge length before and after the tests. Three samples were tested in each cycle. A Buehler MMT-7 was used to test Vickers hardness under a load of 25g for 10 s at ambient temperature.

3. Results and discussion

Figure 2 shows the microstructure of the Al–0.1% (vol) Fe_3O_4 nanocomposites after one ARB cycle. The figure indicates that nanoparticles accumulated in the form of agglomerates and that many free spaces formed between the particles. In the first ARB cycle, the particles were elongated agglomerates that were oriented along the rolling direction (RD) given that the specimens were subjected to rolling. This particle accumulation may be attributed to the distribution of the particles on the surface at the early stage of rolling and the shear stress exerted on the particles. The agglomeration and aggregation of particles in an Al matrix reflect cracks in the matrix and extruded particles. At this stage, agglomeration and aggregation reduce strength because of the three-dimensional tensions occurring in the accumulation of agglomerates. The upshot of this process is the more rapid occurrence of fractures.

Table 1. Specifications of commercial annealed pure Al (Al 1100)

Chemical composition (Wt. %)	Tensile strength (MPa)	Yield strength (MPa)	Elongation (%)
99.9 Al, 0.17 Si, 0.49 Fe, 0.12 Cu, 0.02 Mn, 0.09 others	84.5	39.3	37.8

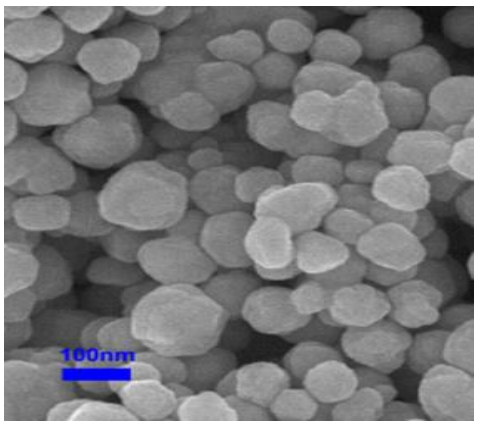

Figure 1. TEM micrograph of spherical Fe_3O_4 particles

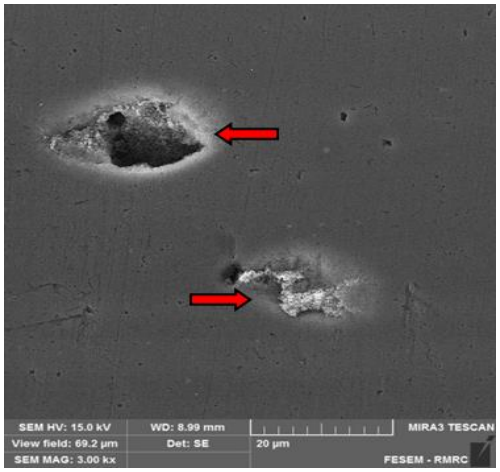

Figure 2. FESEM micrograph of Al–0.1% Fe3O4 after the first ARB cycle

Figure 3 shows the FESEM micrographs and related XRD patterns of the Al–0.1% Fe_3O_4 nanocomposites; these images were taken from the cross-section of the precursor strips after four, six, and eight cycles. Figure 3(a) indicates the connection between Al and iron oxide particles (green arrows), porosity (red circle), and oxide layers that ruptured during rolling (red arrows).

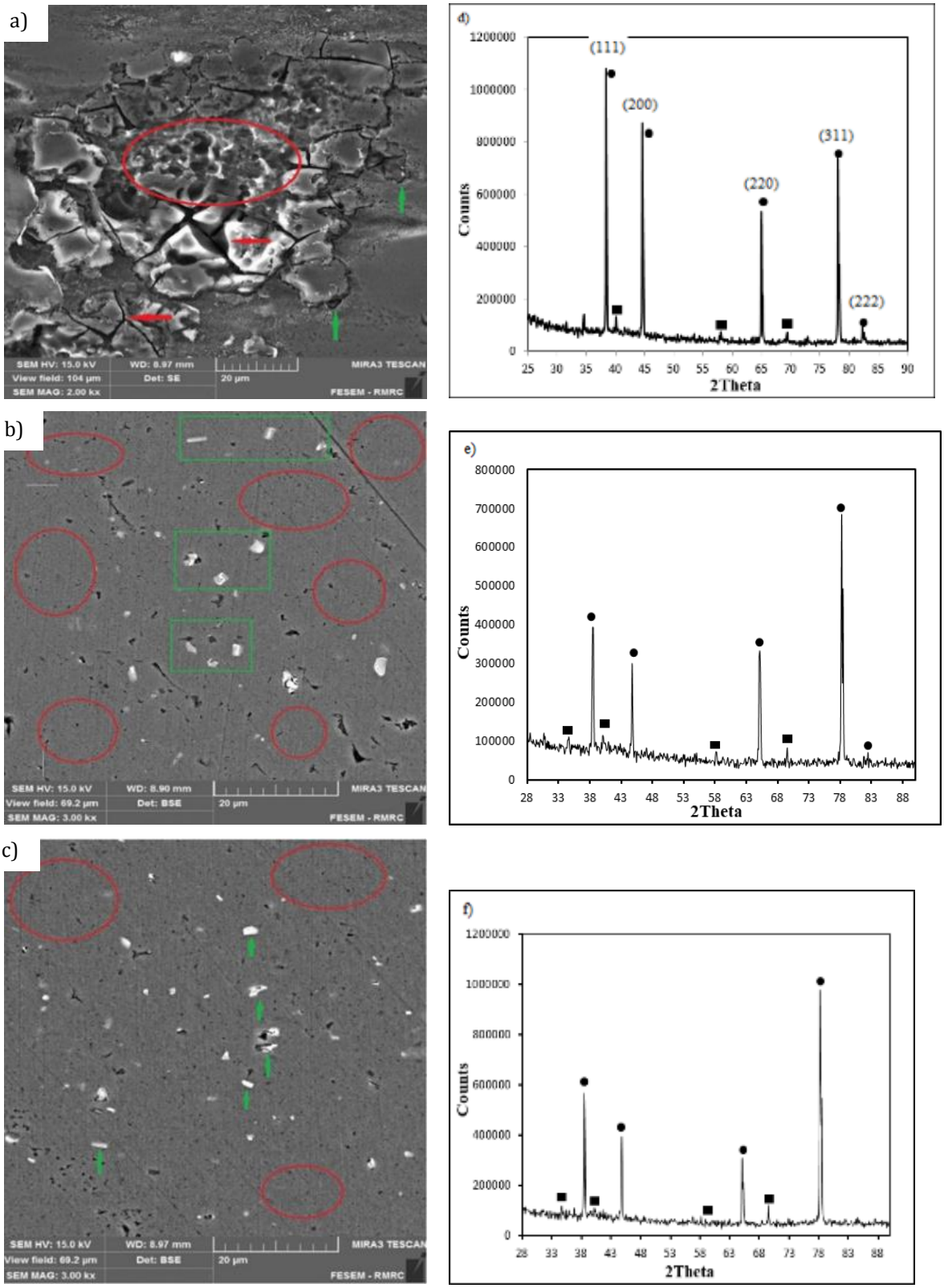

Figure 3. FESEM micrographs and XRD patterns of Al–0.1% Fe3O4 in (a, d) 4, (b, e) 6, and (c, f) 8 cycles of ARB

During rolling and the loading of vertical force, the two oxide layers that formed on surface sheets were broken, and the matrix materials were extruded in the bottom layer. These phenomena caused the clusters and agglomerates to penetrate into the metal matrix, thereby leading to the dispersion of the particles in the matrix, the loss of reinforcement clusters, and increased particle spacing in the clusters [16–18]. However, because of the increase in accumulated particles in the matrix, the aggregation of particles prevented metal–metal extrusion and reduced the adhesion of the two metals. After the sixth cycle (Fig. 3(b)), the particles were randomly distributed in the metal matrix, and the free spaces between the particles decreased and were replaced by clusters. During rolling, increasing elongation along the RD is a function of the extent of reduction of a cross-section, which causes clusters to orient toward the RD and expansion particles to form into clusters. These effects cause clusters to scatter and disperse and then produce a more homogeneous structure.

At a high number of cycles (eight cycles), fewer clusters appeared but more particles dispersed, thereby resulting in more uniform particle distribution. The black areas in the images in Fig. 3 stemmed from particle isolation from the matrix during sample preparation and polishing. Creating a composite with ideal properties requires a high volume fraction of fine particles, and this requirement is associated with difficulties because ultrafine particles tend to cluster and agglomerate. Clustering and agglomeration create a non-uniform structure, and a high volume fraction increases non-uniformity, thus causing a sharp drop in the plasticity and ductility of a composite. The volume fractions of particles and the formation of material defects are directly correlated; defects and cracks form and spread in reinforcement clusters [19, 20]. Thus, a lower volume fraction, a greater number of cycles, and a reinforcement particle size below 100 nm should be adopted to ensure the fabrication of a homogeneous structure in the ARB process [20].

The XRD analysis showed that the main phase present in the nanocomposites was Al, which had a high peak height, and that the partial phases were iron oxide nanoparticles (Fig. 3). No intermetallic phase was produced during the ARB process—a phase stability that is due to a low process temperature. Patterns of Al peaks appeared with varying intensities at different cycles. At four cycles, the peak on plane (111) was the most intense because the slip system of Al with a face centered cubic structure is activated on this plane. In the ARB process, therefore, increased peak intensity can be associated with an increasing number of dislocations on plane (111) and the presence of Fe_3O_4 reinforcement particles as obstacles to movement dislocation. As the number of ARB cycles rises, dislocations develop on the (311) plane, and peak intensity on the (111) plane decreases. This reduction in peak intensity can be caused by the recrystallization that occurs during ARB. As shown in Fig. 3(e), the peak intensity increased on plane (311). Consequently, in the ARB process, which produces UFG structures at a high number of cycles, continuous recrystallization increases the number of misorientation grains [11, 12].

Crystallite size was measured using the Williamson–Hall method on the basis of the XRD data [21]. The peak width indicated a high strain, and a small crystallite size of 198 nm was determined for the Al crystals. In cases wherein plastic deformation occurred in the materials, therefore, the crystallite size obtained from the XRD analysis reflects a dislocation cell or sub-grain [21]. The stress–strain curves of annealed pure Al, ARBed Al, and the Al–0.1% Fe_3O_4 nanocomposites after eight cycles of ARB are illustrated in Fig. 4. The tensile strength of the Al–0.1% Fe_3O_4 nanocomposites increased to as much as 204 MPa, which is 2.4 and 1.14 times the tensile strengths of annealed pure Al and ARBed Al, respectively. This increased strength is ascribed to the uniform dispersion of the reinforcement iron oxide nanoparticles in the matrix, with the particles acting as obstacles to the movement of dislocations.

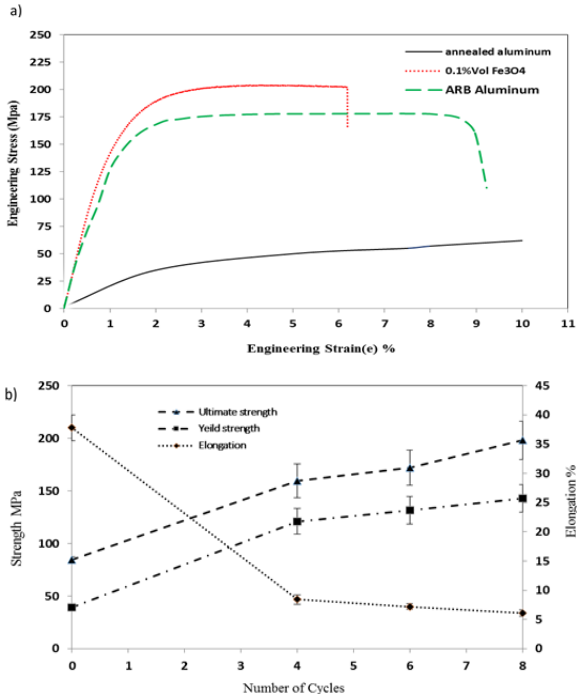

Figure 4. Mechanical properties: (a) Stress–strain curves of annealed Al, ARBed Al, and Al–0.1% Fe_3O_4 produced via ARB after 8 cycles; (b) tensile strength, yield strength, and elongation of the nanocomposite particles as a function of ARB cycle

a)

According to previous studies, parameters such as reinforcement particle size, uniform distribution, and strong connections between reinforcement particles and a metal matrix contribute to dramatic improvements in the physical and mechanical properties of composites [22]. This observation is confirmed in Fig. 4(a). The tensile tension, yield stress, and elongation of the nanocomposites are shown as a function of ARB cycle in Fig. 4(b). Increasing the number of ARB cycles generated a yield strength that was about 300 times higher (i.e., 118 MPa after eight cycles) than that of annealed Al, although the level of strain declined to 8.4%, 7.3%, and 6.1% after four, six, and eight ARB cycles, respectively. The evolution of increasing cycles continued through the increase in work hardening and strength at subsequent cycles, so that the conditions of plastic instability caused by the fine grains that formed during ARB strongly reduced the strain level. This phenomenon continued with a further increase in the number of cycles. The extent of elongation decreased very slightly and remained approximately constant in the final cycles.

Tensile strength also increased as the number of ARB cycles rose, with such strength reaching 160 and 172 MPa in the fourth and sixth cycles, respectively. This increase is due to two factors, as indicated by the Hall–Petch mechanism: the dislocation movement-induced increase in work hardening at early ARB cycles and the formation of fine grains at later ARB cycles [22]. Two mechanisms, namely, the Hall–Petch and Orowan [23] strengthening mechanisms in composites produced via ARB, play an important role in increasing the strength of composites containing reinforcement particles with grain sizes below 1 μm. In the Hall–Petch mechanism, increased strength is associated with grain size, and this relationship is expressed as follows:

$$\sigma_y = \sigma_0 + K_y\, d^{-1/2} \quad (1)$$

where yield strength, material constant, and d (grain size) are linked with the volumetric fractions and sizes of reinforcement particles defined by the Zener equation [24]:

$$d_m = 4\alpha d_p / 3V_p \quad (2)$$

in which d is constant, d_p denotes reinforcement particle size, and V_p represents the volume fraction of particles.

The Orowan mechanism is defined by the movement of dislocations and their pinning with particles. The movement and pinning of dislocations augment the stress imposed on a workpiece. If interparticle spaces decrease and dislocation movement increases in difficulty, more stress is required. The Orowan mechanism is defined according to the following equation [23]:

$$\sigma_{Orowan} = M\, 0.4Gb/\pi(1-\vartheta)^{1/2} \ln(d/b)/\lambda \quad (3)$$

where M is the orientation factor; G denotes the matrix shear modulus Pa; b is Burgers' vector, which indicates the Poisson's coefficient; λ represents the spaces between particles; and d stands for the grain diameter. With Eqs. (1) and (3), strength ratio was 1.1 and 0.26 times higher in eight cycles, which were obtained with the Hall–Petch and Orowan mechanisms, respectively. Strength is calculated using the Clyne equation [25] as follows:

$$\Delta\sigma_{total} = \sqrt{\Delta\sigma_{Hall-Petch}{}^2 + \Delta\sigma_{Orowan}{}^2} \quad (4)$$

The strengthening rate is estimated using the following formula:

$$\Delta\sigma_2 = 1.13\, \Delta\sigma_1 \quad (5)$$

The strengthening value derived in the experiments conducted in this work was 1.22. A comparison of this result with the values obtained on the basis of the Hall–Petch and Orowan mechanisms indicated that the latter mechanism more effectively increased strength. Although there was a slight difference concerning other mechanisms of strengthening, this was negligible and was therefore excluded from the discussion.

Fig. 5(a) displays changes in the microhardness of the Al–0.1% Fe_3O_4 nanocomposites along the RD and normal direction. The microhardness changes were almost uniform in the longitudinal direction but slightly more uniform below the surface layers. The increased microhardness resulted from the shear strain imposed on the surface sheets. Given that ARB is performed without lubrication, friction between rollers and residual shear strain increase on the outer region of a surface, thereby increasing hardness on the surface to a level higher than that observed in other areas of a workpiece [26]. The microhardness of the materials in this work rapidly rose in the first two ARB cycles, reaching 51.5 HV, which is 2.7 times higher than the microhardness of annealed Al. This increase can be attributed to work hardening and the high density of dislocations. The microhardness further increased to 63 HV, which indicates an augmentation of approximately 330% after eight cycles. The sharp rise in microhardness diminished in the middle cycles as a result of inter-reactions among dislocations, dynamic recovery, and recrystallization [27]. Figures 5(b) and 5(c) show the indentation of hardness after two and six cycles, respectively. Because of the movement of dislocations and slip bands, the impact point of hardness penetrated into the samples, creating a sunken-in appearance. With increasing number of cycles, the density of dislocations

decreased, and plastic deformation occurred, thus forming a pile-up point of hardness.

In relevant studies [28], an approximate equation was obtained to calculate the relationship between the ultimate tensile stress (UTS) and hardness as follows [29]:

$$H_V \approx 3\sigma_{UTS} \quad (6)$$

where H_V is the Vickers hardness equal to the UTS.

The theoretical and experimental hardness values of the Al–Fe_3O_4 nanocomposites as a function of the number of ARB cycles are presented in Fig. 6. The curve reflects three outcomes: the hardness was less than the UTS (type I); the hardness was greater than the UTS (type II); and the hardness was equal to the value of the UTS. Naturally, the hardness of annealed materials falls between yield strength and the UTS [29]. During the first cycle (type I), the hardness rapidly increased which, as mentioned earlier, was caused by rising dislocation movement and slip bands. Furthermore, the grains were coarse, and the point of impact easily penetrated into the sample, consequently reducing the practical hardness to a level lower than the theoretical one. The hardness then dramatically increased (type II). In cycles two to five, the effects of the reinforcement nanoparticles with a high strength and hardness were thoroughly visible. The particles acted as a pin against dislocations and increased work hardening. The particle effect gradually diminished in the third zone (type III), and the practical hardness approached the theoretical value. This was caused by the continuous grain recrystallization in the final cycles of ARB.

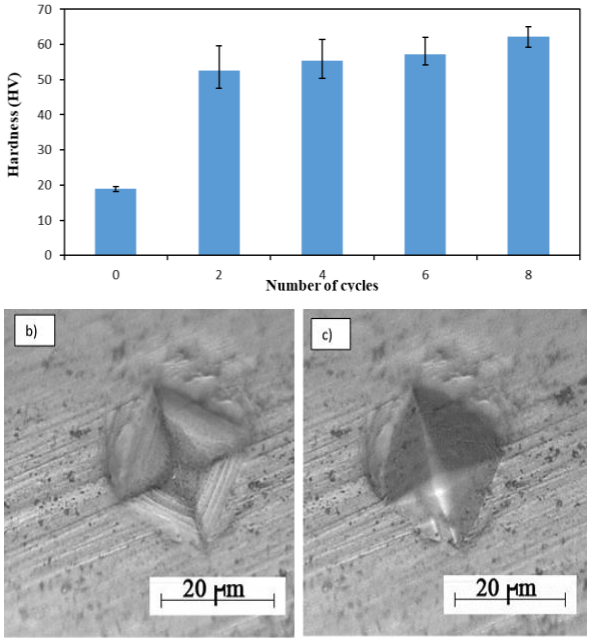

Figure 5. Hardness values of Al–0.1% Fe3O4 at various ARB cycles (a) and indentation of hardness after (b) 2 and (c) 6 cycles

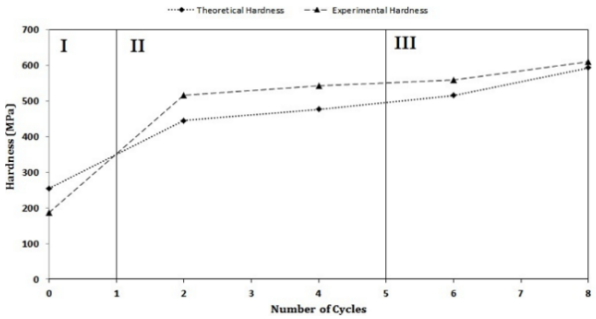

Figure 6. Curves of theoretical hardness and experimental hardness as a function of the number of ARB cycles

Figure 7 depicts the fracture surfaces of the Al–0.1% Fe_3O_4 nanocomposites after four ARB cycles. As presented in Fig. 7(b), voids were created in a direction perpendicular to the rolled plane (slightly toward the transverse direction), and the fracture in the metal matrix occurred because of the ductile rupture mechanism. Around the Fe_3O_4 agglomerates, dimples were less elongated than those observed in another of the specimens (denoted by red circles in Fig. 7(b)), but in another area, the accumulated particles increased and were fully elongated in the RD; ductile rupture also occurred. Figure 7(c) illustrates slip bands, which caused locking between a plate and a slip; this behavior then stopped (green arrow), as can be seen in the interface between the layers of the Al matrix, and then the slip continued in other directions. Microvoids likewise formed because of the particles.

Another ruptured surface is shown in Fig. 7(d), which indicates that slip bands formed on a large scale in the direction of fractures. The rings in the image indicate that the fracture occurred because of the formation of slip bands. Clearly visible in the image are discontinuities at the interface, which are an influencing factor for crack formation and growth and eventual fracture occurrence. The ruptured surfaces of Al–0.1% Fe_3O_4 after six and eight ARB cycles are shown in Fig. 8. The fracture surfaces depict a ductile fracture and ruptured layer with many fine dimples. The rupture occurred because of a crack and its growth in the second phase (reinforcement particles), generating primary microvoids. This microvoid formation was caused by the fact that cohesive traction pulled few particles into the matrix around the microvoids, which expanded with increasing stress and eventually joined. The joining of initial ruptures is associated with two mechanisms, depending on incerement size and interparticle spaces; these mechanisms are initial crack growth, because of the growth and interlocking of voids, and the deformation of slip bands and the relationship between voids [30].

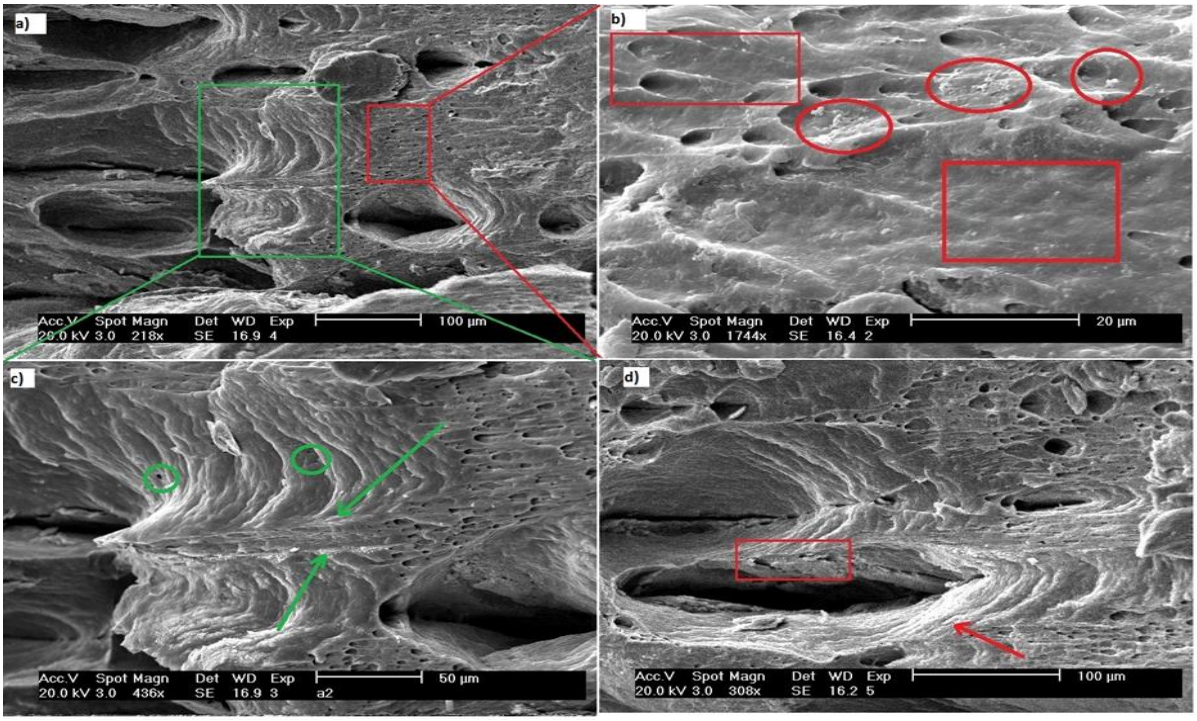

Figure 7. Fractography (different magnifications) of Al–0.1% Fe3O4 nanocomposites at 4 ARB cycles after tensile testing

In the ARB process, particle size decreased with increasing number of cycles, thereby leading to increased initial cracks and a greater number of voids in cycle eight than in cycle. The differences in microvoids can be clearly seen in Figs. 8(a) and 8(b).

The presence of agglomerates and clusters in some areas induced the early formation of cracks with shallow dimples after six cycles [31]. Overall, shallow dimples formed because of more uniform particle distributions and reduced the spaces between the particles (Figs. 8(b) and 8(d)).

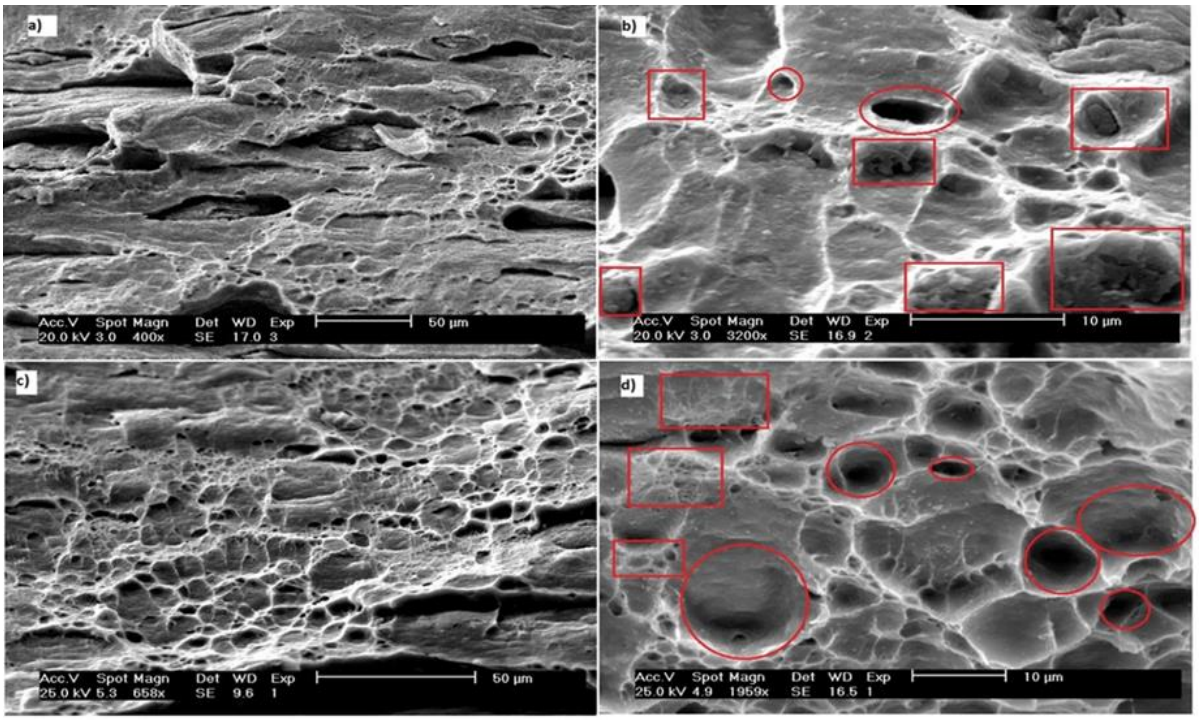

Figure 8. Fractography (different magnifications) of Al–0.1% Fe_3O_4 nanocomposites: (a, b) 6 ARB cycles, (c, d) 8 ARB cycles after tensile testing

4. Conclusion

In this work, ARB was implemented as a new technique of ensuring the uniform distribution of Fe3O4 particles in an Al matrix. The results are summarized as follows:

1. After four cycles, particles randomly dispersed and generated particle-free zones in the specimens. Increasing the number of ARB cycles to eight reduced agglomerations and created a more uniform distribution of particles.

2. Increasing the number of ARB cycles improved the tensile strength of the Al–0.1% Fe3O4 by 2.4 times that of annealed Al. It reached 204 MPa after eight cycles, during which yield strength also increase to 118 MPa. The Hall–Petch and Orowan mechanisms played an important role in the strengthening of the nanocomposites.

3. The hardness of the Al–0.1% Fe3O4 nanocomposites increased to 63 HV after eight cycles—a value that reflects an almost 330% increase. The experimental and theoretical hardness values were close after eight cycles, indicating that the inherent properties of the nanocomposites improved.

4. Surface fractures showed that the fracture mechanism acting on the nanocomposites was a ductile rupture. Increasing the number of ARB cycles caused particles to disperse in a uniform manner and augmented the number of shallow voids.

Acknowledgements

The authors would like to thank Semnan University for partially providing laboratory facilities.

References

[1] Zhang Z, Chen DL. Contribution of Orowan strengthening effect in particulate-reinforced metal matrix nanocomposites. *Material Science Engineering A* 2008; 483–484: 148–152.

[2] Baazamat S, Tajally M, Borhani E. Fabrication and characteristic of Al-based hybrid nanocomposite reinforced with WO_3 and SiC by accumulative roll bonding process. *Journal of Alloys and Compounds* 2015; 653: 39-46.

[3] Luo P, McDonald DT, Xu W, Palanisamy S, Dargusch MS, Xia K. A modified Hall–Petch relationship in ultrafine-grained titanium recycled from chips by equal channel angular pressing. *Scripta Mater* 2012; 66: 785–788.

[4] Rezaei MR, Toroghinejad MR, and Ashrafizadeh F. Effects of ARB and Ageing Processes on Mechanical Properties and Microstructure of 6061 Aluminum Alloy. *Journal of Materials Processing Technology* 2011; 211: 1184-1190.

[5] Toptan F, kilicarslan A, Karaaslan A, Cigdem M, Kerti I. Process and microstructural characterization of AA 1070 and AA 6063 matrix B_4C reinforced composites. *Materials and Design* 2010; 31: 87-91.

[6] Borhani E, Jafarian H, Terada D, Tsuji N. Microstructural Evolution during ARB Process of Al-0.2 %mass SC Alloy Containing Al_3Sc Precipitates in Starting Structures. *Materials Transactions* 2012; 53: 72-80.

[7] Borhani E, Jafarian H, Shibata A, Tsuji N. Texture Evolution in Al-0.2 mass% SC Alloy during ARB Process and Subsequent Annealing. *Materials Transactions* 2012; 53: 1863-1869.

[8] Borhani E, Jafarian H, Adachi H, Terada D, Tsuji N. Annealing Behavior of Solution Treated and Aged Al-0.2 wt% Sc Deformed by ARB. *Materials Science Forum* 2010; 667: 211-216.

[9] Salimi A, Borhani E, Emadoddin E. Evaluation of mechanical properties and structure of 1100-Al reinforced with ZrO_2 nano-particle via accumulatively roll-bonded. *Procedia Materials Science* 2015; 11: 67-73.

[10] Jamaati R, Toroghinejad MR, Dutkiewicz J, Szpunar JA. Investigation of nanostructured Al/Al_2O_3 composite produced by accumulative roll bonding process. *Materials and Design* 2012; 35: 37-42.

[11] Alizadeh M, Paydar MH. Fabrication of Al/SiCp composite strips by repeated roll-bonding (RRB) process. *Alloys and Compounds* 2009; 477: 811-816.

[12] Katundi D, Ayari F, Bayraktar E, Tan MJ, Touson Bayraktan A. Design of aluminum matrix composite reinforced with nano iron oxide (Fe3O4). In: 15th international conference on advance material processing technologies Australia; 2012. p. 1-12.

[13] Asif M, Chandra K, Misra PS. Development of aluminum based hybrid metal matrix, composites for heavy duty application. *Miner Mater Character Eng.* 2011; 10(14): 1337-1344.

[14] Katurdi D, Ayari F, Bayraktar E, Tan MJ, Touson Bayraktan A. Manufacturing of aluminum matrix composite reinforced with iron oxide (Fe3O4) nanoparticle, microstructure and mechanical properties. *Metallur Mater Trans B* 2013; 45(2): 352-362.

[15] Bayraktar E, Katundi D. Development of a new aluminum matrix composite reinforced with iron oxide (Fe3O4). *AChiev Mater Manuf Eng.* 2010; 38(1): 7-14.

[16] Clyne TW, Withers PJ. An Introduction to Metal Matrix Composites. Cambridge: Cambridge University Press; 1993.

[17] Alizadeh M. Processing of Al/B_4C Composites by Cross-Roll Accumulative Roll Bonding. *Materials Letters* 2010; 64: 2641-2643.
[18] Li L, Nagai K, Yin F. Progress in cold roll bonding of metals. *Sci. Technol. Adv. Mater* 2008; 9: 023001.
[19] Bay N. Mechanisms producing metallic bonds in cold welding. *Welding J.* 1983; 62(5): 137.
[20] Jamaati R, Toroghinejad MR. Investigation of the parameters of the cold roll bonding (CRB) process. *Materials Science and Engineering A* 2010; 527(9): 2320-2326.
[21] Lloyd DJ. Aspects of fracture in particulate reinforced metal matrix composite. *Acta Metallurgica et Materialia* 1991; 42: 59-71.
[22] Reihanian M, Bagherpour E, Paydar MH. On the achievement of uniform particle distribution in metal matrix composite fabricated by accumulative roll bonding. *Materials letters* 2013; 91: 59-62.
[23] Sanaty-Zadeh A. Comparison between current models for the strength of particulate-reinforced metal matrix nanocomposites with emphasis on consideration of Hall–Petch effect. *Materials Science and Engineering A* 2012; 531: 112– 118.
[24] Zener C, Smith CS. Grains phased and interface: an interpretation of microstructure. *Trans AIME* 1948; 175: 15-51.
[25] Clyne TW, Hall D. An introduction to composite materials, Part of Cambridge Solid State Science Series. 2nd Edition; 1996.
[26] Hanazaki K, Shigeiri N, Tsuji N. Change in Microstructures and Mechanical Properties during Deep Wire Drawing of Copper. *Materials Science and Engineering A* 2010; 527: 5699-5707.
[27] Alizadeh M, Paydar MH, and Sharifian Jazi F. Structural Evaluation and Mechanical Properties of Nanostructured Al/B_4C Composite Fabricated by ARB Process. *Composites Part B: Engineering* 2013; 44: 339-343.
[28] Boyer HE, Gall TL. Metals Handbook, Desk Edition, ASM International, Metals Park, Ohio; 1985.
[29] Zhang P, Li SX, Zhang ZF. General relationship between strength and hardness. *Materials Science and Engineering A* 2011; 529: 62-73.
[30] Becker W, Lampman S. Fracture appearance and mechanisms of deformation and fracture, Materials Park, OH: ASM International; 2002.
[31] Eizadjou M, Kazemi Talachi A, Danesh Manesh H, Shakur Shahabi H, Janghorban K. Investigation of structure and mechanical properties of multi –layers Al/Cu composite produced by accumulative Roll Bonding (ARB) Process. *Composite Science and Technology* 2008; 68: 2003-2009.